Tensions on the actin cytoskeleton and apical cell junctions in the *C. elegans* spermatheca are influenced by spermathecal anatomy, ovulation state and activation of myosin

Fereshteh Sadeghian[1], Noa W. F. Grooms[1], Samuel H. Chung[1] and Erin J. Cram[2]*

[1]Department of Bioengineering, Northeastern University, Boston, MA, United States, [2]Department of Biology, Northeastern University, Boston, MA, United States

Introduction: Cells generate mechanical forces mainly through myosin motor activity on the actin cytoskeleton. In *C. elegans*, actomyosin stress fibers drive contractility of the smooth muscle-like cells of the spermatheca, a distensible, tube-shaped tissue in the hermaphrodite reproductive system and the site of oocyte fertilization. Stretching of the spermathecal cells by oocyte entry triggers activation of the small GTPase Rho. In this study, we asked how forces are distributed *in vivo*, and explored how spermathecal tissue responds to alterations in myosin activity.

Methods: In animals expressing GFP labeled actin or apical membrane complexes, we severed these structures using femtosecond laser ablation and quantified retractions. RNA interference was used to deplete key contractility regulators.

Results: We show that the basal actomyosin fibers are under tension in the occupied spermatheca. Reducing actomyosin contractility by depletion of the phospholipase C-ε/PLC-1 or non-muscle myosin II/NMY-1, leads to distended spermathecae occupied by one or more embryos, but does not alter tension on the basal actomyosin fibers. However, activating myosin through depletion of the Rho GAP SPV-1 increases tension on the actomyosin fibers, consistent with earlier studies showing Rho drives spermathecal contractility. On the inner surface of the spermathecal tube, tension on the apical junctions is decreased by depletion of PLC-1 and NMY-1. Surprisingly, when basal contractility is increased through SPV-1 depletion, the tension on apical junctions also decreases, with the most significant effect on the junctions aligned in perpendicular to the axis of the spermatheca.

Discussion: Our results suggest that much of the tension on the basal actin fibers in the occupied spermatheca is due to the presence of the embryo. Additionally,

increased tension on the outer basal surface may compress the apical side, leading to lower tensions apically. The three dimensional shape of the spermatheca plays a role in force distribution and contractility during ovulation.

1 Introduction

Mechanical forces regulate essential cellular processes such as adhesion, signaling, proliferation, and differentiation. Throughout morphogenesis, mechanical forces alter cell shapes (Fischer et al., 2014). Cells generate mechanical forces predominantly through the action of the motor protein myosin on the actin cytoskeleton (Fischer et al., 2014; Amiri et al., 2023). The actin cytoskeleton is a dynamic network formed by the polymerization of globular actin monomers (G-actin) into helical filaments (F-actin). Actin networks

FIGURE 1
Structure of the spermatheca. **(A)** Brightfield image of an adult hermaphrodite false colored to indicate the sheath cells (yellow), spermathecae (green), uterus (blue), and gut (red). **(B)** Diagram of the area indicated by a black box in A during an ovulation. First panel: sheath cell contractions begin to push the proximal oocyte (white). Second panel: sheath contractions force the oocyte into the spermatheca, where it is fertilized. Used by permission (Wirshing and Cram, 2018). Third panel: the spermathecal-uterine valve opens as the spermathecal bag contracts to expel the fertilized embryo into the uterus. Insert in **(B)** shows a magnified cross-section of the spermatheca indicating that the apical surface faces the lumen. Scale bars, 50 μm in **(A)** and 20 μm in **(B)**. **(C)** Unoccupied spermatheca showing green actin ACT-1::GFP and red gap junction INX-12::mApple expression before oocyte entry. **(D)** Occupied spermatheca showing aligned green actin and red gap junctions during ovulation. **(E)** Diagram of the spermatheca indicating basal actin in green and apical membrane in red, indicating the membranes parallel and perpendicular to the axis of spermatheca. Created with Biorender.com. **(F)** Basal Actin/ACT-1::GFP and Apical junction/AJM-1::RFP expression in spermatheca. **(G)** A cross section of the same spermatheca in **(F)** showing green basal actin on the exterior surface and red apical membrane on the interior surface. Scale bar, 20 μm.

are crucial for various cellular processes such as cell migration, tissue morphogenesis, wound healing, and the adaptation of cells and tissues to physical stress (Kelley and Cram, 2019). Stress fibers are contractile actomyosin bundles, commonly found in cells experiencing physical stress (Kelley and Cram, 2019). Cells use actomyosin stress fibers to exert traction forces against focal adhesions, integrin-based adhesive structures that link the cytoskeleton to the extracellular matrix (ECM) (Kassianidou et al., 2017).

To study coordinated actomyosin contractility in an intact context, we use the *Caenorhabditis elegans* reproductive system as a model. The hermaphrodite gonad consists of two symmetrical gonad arms containing germ cells and oocytes surrounded by sheath cells, two spermathecae, and a common uterus (Figure 1A) (Castaneda et al., 2020). The spermatheca, which stores sperm and serves as the site of fertilization in the hermaphrodite, is a contractile tube comprising 24 smooth muscle-like cells. The spermathecal-uterine (sp-ut) valve is a contractile sphincter that connects the spermatheca to the uterus. The apical surface of the spermatheca faces the oocyte. Upon the entry of the oocyte (Figure 1B), immediate fertilization occurs, initiating the formation of the eggshell. Subsequently, the spermatheca undergoes coordinated contractions to propel the embryo through the sp-ut valve and into the uterus (Kelley et al., 2020).

Stress fiber-like bundles of actin and myosin drive spermathecal contractility (Kelley and Cram, 2019). These bundles are on the outer, basal surface of the spermathecal cells and in most spermathecal cells are aligned perpendicular to the axis of the spermatheca (Kelley and Cram, 2019). The inner, luminal sides of the cells are connected by apical cell-cell junctions (Wirshing and Cram, 2018). Prior to oocyte entry, the spermatheca is relaxed and compact (Figure 1C); during ovulation cells are stretched by the presence of oocyte (Figure 1D). The diagram in Figure 1E depicts the spermathecal anatomy with basal actin fibers and the interior apical junctions. Figure 1F gives the exterior view, and Figure 1G gives the interior view of the occupied spermatheca, with red apical junctions and green basal actin.

The contraction of actomyosin fibers in the spermatheca is regulated by highly conserved pathways similar to non-muscle and smooth muscle cell cascades (Castaneda et al., 2020). Briefly, activation of the phospholipase PLCε/PLC-1 leads to cleavage of the membrane lipid PIP_2, resulting in the production of IP_3 (Castaneda et al., 2020). Binding to the IP_3 receptor triggers the release of Ca^{2+} from the endoplasmic reticulum and subsequent activation of the myosin light chain kinase/MLCK-1 (Wirshing and Cram, 2017). In a parallel pathway, oocyte entry causes displacement of the RhoGAP SPV-1, activating RhoA/RHO-1 and ROCK/LET-502 (Bouffard et al., 2019). This activation leads to the phosphorylation and activation of non-muscle myosin II/NMY-1, resulting in the contraction of actomyosin fibers (Castaneda et al., 2020). Activation and coordination of both pathways is necessary for embryos to successfully pass through the spermatheca. SPV-1, a BAR-domain-containing Rho GAP, functions as a tension sensor in the spermatheca, localizing to low-tension membranes where it maintains Rho/RHO-1 in an inactive state (Tan and Zaidel-Bar, 2015). Prior to the first ovulation, the spermathecal actin forms a diffuse, weblike-network (Kelley and Cram, 2019; Wirshing and Cram, 2017). Activation of myosin pulls the actomyosin fibers into

aligned, parallel arrays (Wirshing and Cram, 2017). For productive contractility, the fibers must be anchored. Filamins form a resilient three-dimensional network of the actin cytoskeleton and establish links between the cytoskeleton and transmembrane proteins, including integrins (Kovacevic and Cram, 2010). Filamin/FLN-1 is essential for anchoring actin bundles at the basal surface of the spermatheca, and preventing the aggregation of actin and myosin near the nucleus (Kelley et al., 2020).

Observation of the actin cytoskeleton during ovulation led us to the hypothesis that the parallel arrays of actomyosin fibers are under tension and that activating myosin would lead to an increase in tension, productive contraction of the spermatheca, and expulsion of the embryo into the uterus. Exit of the embryo from the spermatheca requires coordinated contraction of the distal spermathecal cells (near the entry neck) and dilation of the sp-ut valve (Bouffard et al., 2019). We wondered whether mechanical tension, or increased tension, on the fibers or the cell-cell junctions might provide temporal or positional information to regulate spermathecal contractility or embryo exit. To explore these ideas, we needed to first determine whether the fibers and/or cell junctions are under tension and, if so, whether the perpendicular or parallel junctions might be under higher load.

The mechanical characteristics of actomyosin stress fibers, epithelial cell–cell junctions, and other cellular structures can be explored using laser ablation (Taneja et al., 2020). Femtosecond laser ablation enables minimally invasive disruption of cellular structures with sub-micrometer resolution (Chung et al., 2006; Wang et al., 2022). Laser ablation has been used for studying the viscoelastic response of myofibrils of iPSC-derived cardiomyocyte (Taneja et al., 2020), force transmission between apical and basal nucleus by actomyosin dynamics in *Drosophila* (Ambrosini et al., 2019), and tension in cell-cell boundaries in *Drosophila* follicular epithelium (Mateos et al., 2020) and the amnioserosa (Colombelli and Solon, 2013).

In this study, we employed imaging, laser ablation, and quantitative image analysis to characterize the tensions in the spermatheca. We demonstrate that decreasing actomyosin contractility through depletion of phospholipase C-ε/PLC-1, or non-muscle myosin II/NMY-1, did not alter tension on the basal actomyosin fibers, suggesting much of the tension is coming from the presence of the embryo, at least in the central spermathecal cells and at the timepoint selected. Activating myosin through depletion of the Rho GAP SPV-1 does increase tension on the basal actomyosin fibers. Conversely, increasing contractility through SPV-1 depletion decreased tension on the apical junctions, suggesting that tension on the outer, basal surface of this tubular structure might compress the apical side.

2 Materials and methods

2.1 Strains and culture

Nematodes were grown on nematode growth media (NGM) [0.107 M NaCl, 0.25% wt/vol Peptone (Fischer Science Education), 1.7% wt/vol BD Bacto-Agar (FisherScientific), 0.5% Nystatin (Sigma), 0.1 mM $CaCl_2$, 0.1 mM $MgSO_4$, 0.5% wt/vol cholesterol, 2.5 mM KPO_4] and seeded with *E. coli* OP50 using standard

C. elegans techniques. Nematodes were cultured at 23°C for 52–72 h (Castaneda et al., 2020). Lines expressing ACT-1::GFP (UN1502) and AJM-1::GFP (UN2140) were previously generated by injecting plasmids and following integration (Kelley et al., 2020; Kelley et al., 2018). Strains used to show the basal and apical side in Figure 1 were generated by crossing ACT-1::GFP and INX-12::mApple (UN1617), ACT-1::GFP and AJM-1::RFP (UN1936).

2.2 RNA interference

The RNAi protocol was performed essentially as described in Kelley et al. (2018). HT115 (DE3) bacteria (RNAi bacteria) transformed with a dsRNA expression construct of interest was grown overnight in Luria Broth (LB) supplemented with 40 µg/mL ampicillin and seeded (150 µL) on NGM plates supplemented with 25 µg/mL carbenicillin and 1 mM disopropylthio-β-galactoside (IPTG). Seeded plates were left for 24–72 h at room temperature (RT) to induce dsRNA expression. Empty pPD129.36 vector ("Control RNAi") was used as a negative control in all RNAi experiments (Castaneda et al., 2020). Embryos from gravid adults were collected using an alkaline hypochlorite solution as described by Hope (1999) and washed three times in M9 buffer (22 mM KH_2PO_4, 42 mM $NaHPO_4$, 86 mM NaCl, and 1 mM $MgSO_4$) ("egg prep"). Clean embryos were transferred to supplemented IPTG plates seeded with HT115 (DE3) bacteria expressing dsRNA of interest and left to incubate at 23°C for 50–56 h depending on the experiment (Castaneda et al., 2020).

2.3 Population assay

Embryos collected via an "egg prep" as previously described were plated on supplemented NGM-IPTG plates seeded with RNAi bacterial clones of interest. Plates were incubated at 23°C for 54–56 h or until animals reached adulthood. Upon adulthood nematodes were killed in a drop of 0.08 M sodium azide (NaAz) and mounted on 2% agarose pads to be visualized using a 60x oil-immersion objective with a Nikon Eclipse 80i epifluorescence microscope equipped with a Spot RT3 CCD camera (Diagnostic instruments; Sterling Heights, MI, United States). Animals were scored for the presence or absence of an embryo in the spermatheca.

2.4 Fluorescence microscopy image acquisition and processing

For time-lapse imaging of ovulation and observations of live or fixed animals, partially synchronized populations were obtained by egg prep and animals were grown at 23°C for ~54 h, around the time of the first ovulation. Live animals were immobilized with 1.85% formaldehyde in PBS for 25 min at room temperature, washed twice in PBS and mounted on a 3% agarose pad. Confocal microscopy was performed on an LSM 710 confocal microscope (Zeiss) equipped with Zen software (Zeiss) using a Plan-Apochromat 63x/1.40 oil DIC M27 objective. A 488-nm laser was used for GFP and DyLight 488, and a 561 nm laser was used for RFP and TexasRed (Kelley et al., 2018).

2.5 Laser severing

A Yb-doped diode-pumped solid-state laser (Spectra-Physics Spirit-1040-4W) outputs 1040-nm 400-fs pulses with a variable repetition rate, set to 1 kHz. We focused laser pulses with a Nikon CFI Plan Apo Lambda 1.4 NA 60× oil immersion objective. We set the laser power to 150 µW (Wang et al., 2022).

2.6 Statistics

Either a Fishers exact *t*-test (two dimensional ×2 analysis) or a one-way ANOVA with a multiple comparison Tukey's test were conducted using GraphPad Prism on total. For population assays, statistics were performed using the total number of unoccupied spermathecae compared with the sum all other phenotypes. N is the total number of spermathecae counted. Fisher's exact *t*-test were used for population assays. Stars designate statistical significance (****$p < 0.0001$, ***$p < 0.005$, **$p < 0.01$, *$p < 0.05$). Non-linear regression analysis was used to show correlation between the length of retraction and the length or width of the spermatheca.

3 Results

3.1 Basal actomyosin fibers in the spermatheca are under tension

The spermatheca expands upon oocyte entry and contracts when the embryo is expelled into the uterus (Figure 1). We have shown that oocyte entry stimulates the rearrangement of the cytoskeleton into parallel, aligned actomyosin bundles on the basal surface of the spermatheca (Kelley et al., 2020) (Figure 1). As described above, spermathecal contractility is regulated by two parallel pathways, one which requires the phospholipase PLC-1/PLCε for calcium release and the other that requires the small GTPase RHO-1/Rho (Castaneda et al., 2020). We have shown previously that *plc-1* and *nmy-1* are required for successful transit of the embryo through the spermatheca (Castaneda et al., 2020; Kelley et al., 2020). Failed transits lead to an increase in the percentage of spermathecae occupied by an embryo. To establish that the conditions to be used in our laser severing experiments do disrupt spermathecal contractility, and to confirm these prior results, we determined the spermathecal occupancy in each RNAi condition and found that, as expected, depletion of *plc-1* and *nmy-1* lead to 100% and 90% occupancy compared to control (empty vector), respectively (Figure 2A).

We also determined whether the depletion of *plc-1* and *nmy-1* led to the expected effects on the actin cytoskeleton (Figure 2). As expected, PLC-1 plays a minor role in the formation of the parallel fiber bundles (Figure 2C) (Kelley et al., 2018) whereas *nmy-1*/myosin depletion results in the failure to form parallel, aligned fiber bundles (Figure 2F). FLN-1/filamin is essential for the development and stabilization of a regular arrangement of parallel, contractile actomyosin fibers in the spermatheca (Kelley et al., 2020). As expected, depletion of FLN-1 disrupts anchoring of fibers in the actin network, leading to an inability to contract (Figure 2E). This
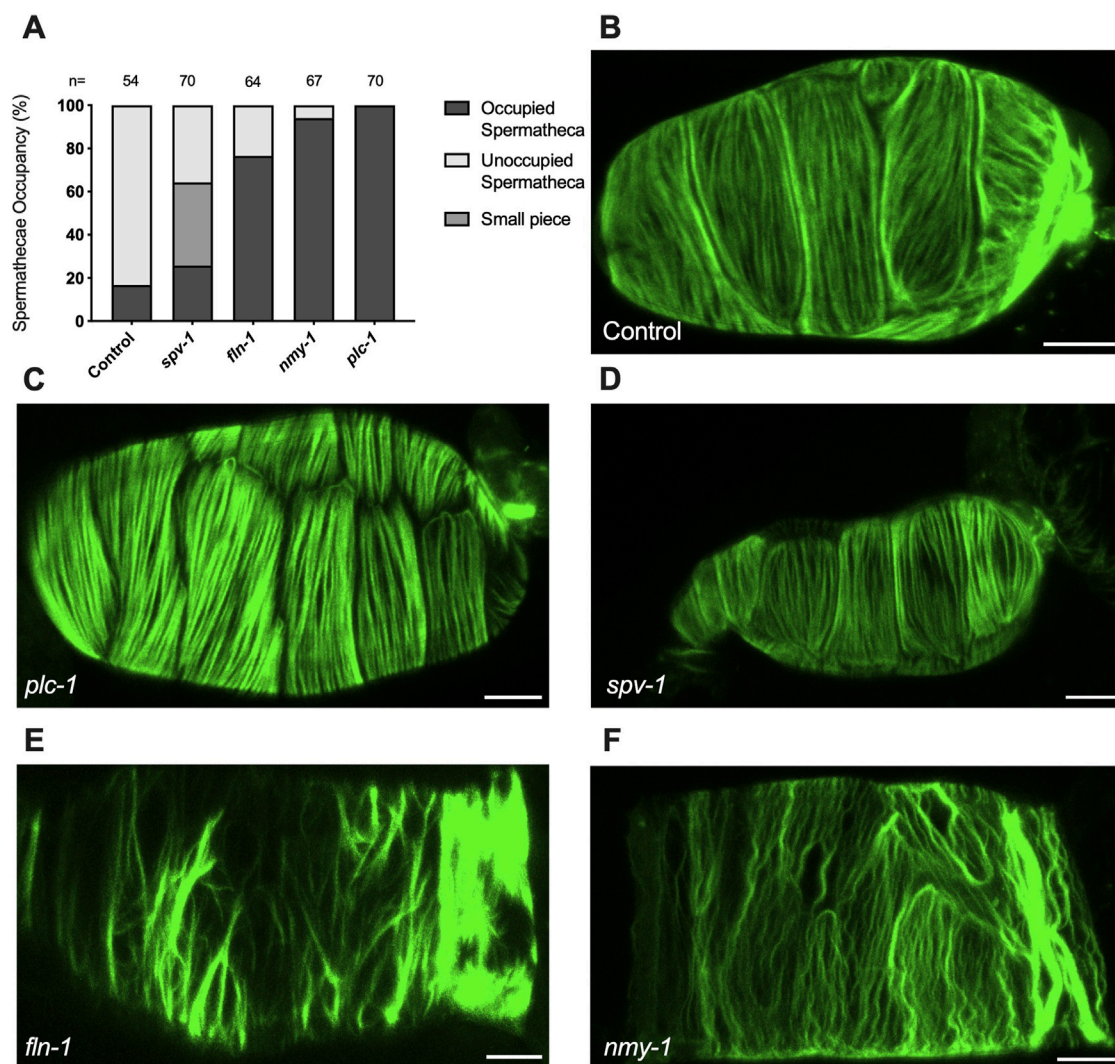
FIGURE 2
Myosin activity is required to for transit through the spermatheca and for the proper organization of F-actin bundles in the spermatheca **(A)** Spermathecal occupancy in wild type ACT-1::GFP animals cultivated on control, *plc-1* RNAi, *spv-1* RNAi, *fln-1* RNAi, and *nmy-1* RNAi. N represents the total number of spermathecae counted. Actin phenotype of wild type animals (ACT-1::GFP) grown on control **(B)**, *plc-1* RNAi **(C)**, *spv-1* RNAi **(D)**, *fln-1* RNAi **(E)**, and *nmy-1* RNAi **(F)**. Scale bar, 20 μm.

defect also results in the trapping of oocytes in the spermatheca (Kelley et al., 2020).

We reasoned that the presence of the embryo exerts tension on the fibers, and that activation of myosin would further increase the tension on the fibers, eventually leading to expulsion of the embryo from the spermatheca. To explore these ideas, we used laser severing to cut basal actin fibers in animals expressing ACT-1::GFP in the spermatheca. The movement of GFP-labeled actin fibers was tracked for up to 30 s after ablation from the point of surgery (Supplementary Movies S1, S2). The traction per second for the first 10 s of each retraction is shown in Figure 3D–G. The actomyosin fibers appear to retract rapidly and then plateau in all conditions. The average total retraction for each is shown in Supplementary Figure S2A.

The actin fibers in the central cells of the spermatheca are aligned circumferentially to the axis of the spermatheca (as shown in Figure 1). All incisions were executed perpendicular to

the axis of the spermatheca. Fiber retraction was normalized to the length of the fiber in all conditions (Figures 3C, 5C–E). The length of retraction after ablation was measured [Supplementary Figure S2A (actin) and Supplementary Figures S2B–D (membrane)]. Then, because the size of spermatheca was different for each condition, the length of the retraction was normalized to the initial length of the corresponding fiber before incision. In some laser ablations, more than one actin fiber was severed in an incision, in this case, the center expansion of the lesion was measured.

To confirm that the fibers were severed, rather than photobleached, we tracked fluorescence recovery after laser ablation, and verified no recovery of the GFP signal in the 30 s following the incision in analysis. To determine whether the fibers depolymerized, rather than retracting, we investigated the length of initial retraction and the following retraction of the severed fibers throughout the time (Figure 3). In four animals, the ablated actin fibers continued to shorten at a slower rate after the initial retraction.
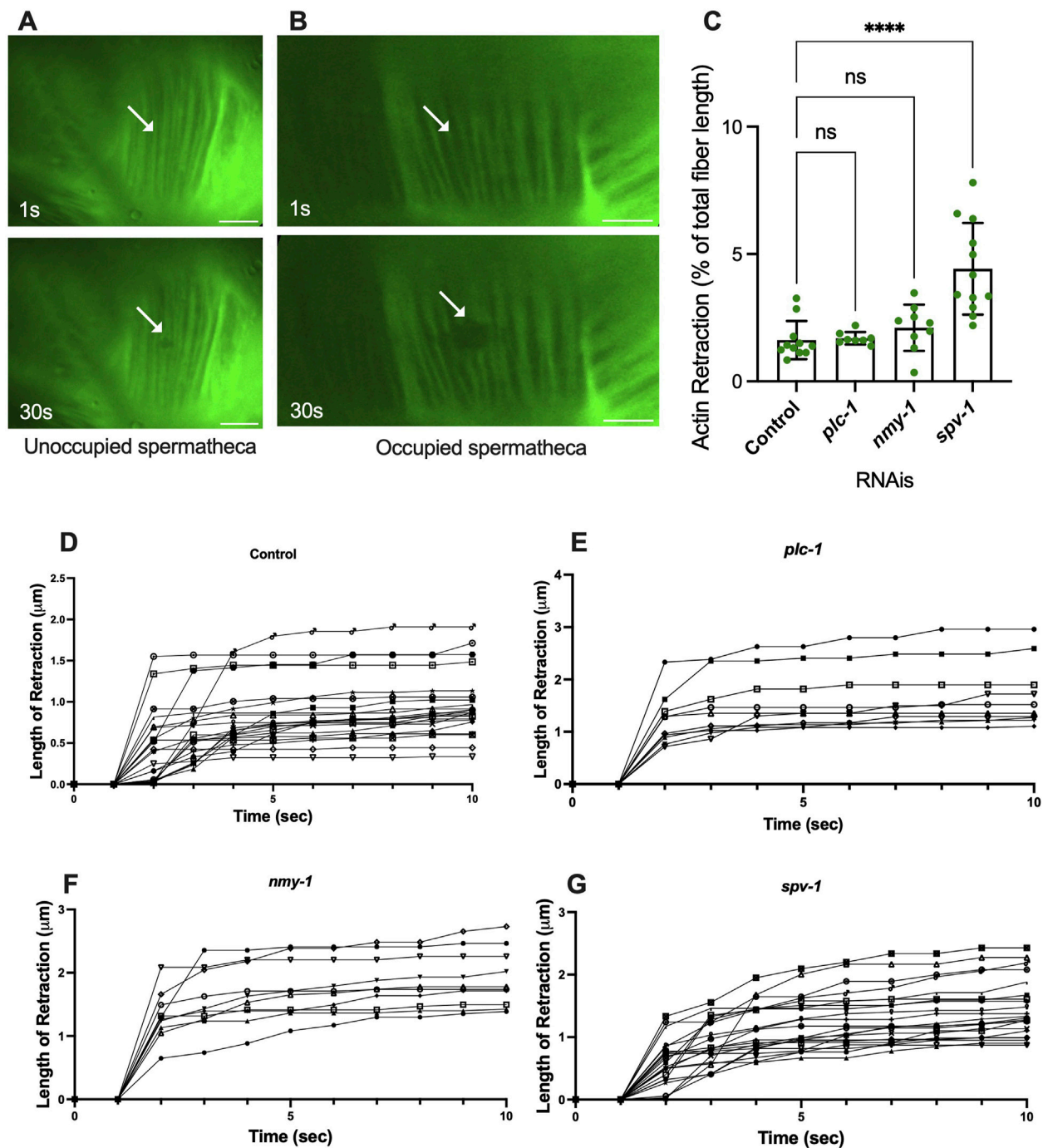
FIGURE 3
Spermathecal occupancy results in increased actin fiber retraction. Laser ablation of ACT-1::GFP expressing animals treated with control RNAi, in the unoccupied spermatheca **(A)**, and occupied spermatheca **(B)** before and 30 s after surgery, (see *plc-1*, *nmy-1*, and *spv-1* RNAis in Supplementary Figure S1). Actin fibers severed using a femtosecond laser. **(C)** Total retraction of actin fibers in control (empty vector), *plc-1*, *nmy-1*, and *spv-1* RNAi. Data indicates higher tension in *spv-1* RNAi treated animals with no significant differences between empty, *plc-1*, and *nmy-1* RNAi treatments. Retraction of control compared to other conditions was conducted using Ordinary one-way ANOVA, ****$p < 0.0001$. **(D–G)** Analysis of length of retraction to the length of the fiber shows tension release of actin fibers after laser ablation in ACT-1::GFP expressing animals treated with control **(D)**, *plc-1* RNAi **(E)**, *nmy-1* RNAi **(F)**, and *spv-1* RNAi **(G)**. Scale bar, 10 µm.

These were excluded from further analysis. All retraction data is shown in Supplementary Figure S2.

To determine whether fiber retraction is influenced by the presence of an oocyte in the spermatheca, we severed fibers in occupied and unoccupied spermathecae. This was challenging in the unoccupied spermatheca, given the folded morphology of the unoccupied tissue (Figure 3A). In unoccupied spermatheca, the ablated area expands from 0.2 µm to 0.4 µm (Figure 3A). This is in contrast to the significant retraction observed in occupied spermatheca under the same severing conditions (Figure 3B), on average from 0.2 µm to 2 µm in occupied
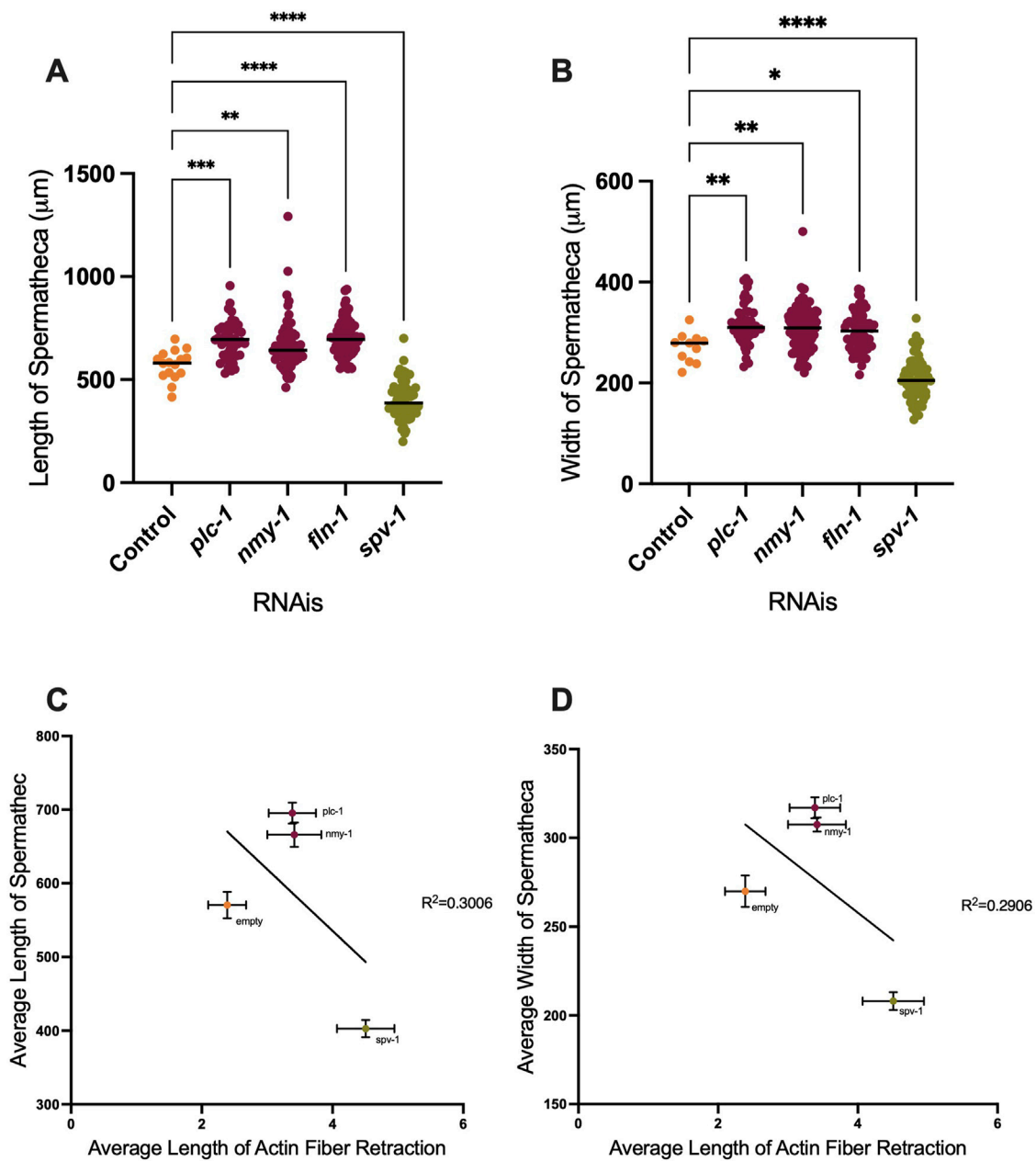
FIGURE 4
Depletion of contractility regulators affects spermathecal dimensions. Length and width of spermatheca of ACT-1::GFP **(A, B)**. **(C, D)** Correlation between length **(C)** and width **(D)** of spermatheca to the length of retraction. Average of actin retraction to the average of length and width of spermatheca is shown for control, *plc-1* RNAi, *nmy-1* RNAi, and *spv-1* RNAi conditions. Non-linear regression analysis was used to assess correlation. Length of control (empty vector) compared to other conditions analyzed by using Ordinary one-way ANOVA, *****p < 0.0001*. Scale bar 20 μm.

controls. This suggests that retraction depends on the presence of the oocyte in the spermatheca, and that the basal fibers are under tension in the occupied spermatheca.

3.2 SPV-1 depletion increases tension on basal actomyosin fibers in spermatheca

We hypothesized that decreasing contractility would decrease the tension on the actin fibers, and increasing contractility would increase tension. To test this, we treated the ACT-1::GFP animals

with control RNAi, *plc-1* RNAi, *nmy-1* RNAi to decrease contractility, and severed actin fibers in occupied spermathecae. To our surprise, inhibiting actomyosin contractility did not affect the tension on the fibers. Following the incision, the actin retracted to the same extent as controls in *plc-1* and *nmy-1* depleted cells (Figure 3C). Because reducing actomyosin contractility does not affect the measured tensions, this suggests most of the tension may come from the presence of the embryo at least in the central cells of the spermatheca and at the timepoint chosen.

We next asked if increasing contractility would increase the tension on the actin fibers. The RhoGAP SPV-1 inactivates RHO-1
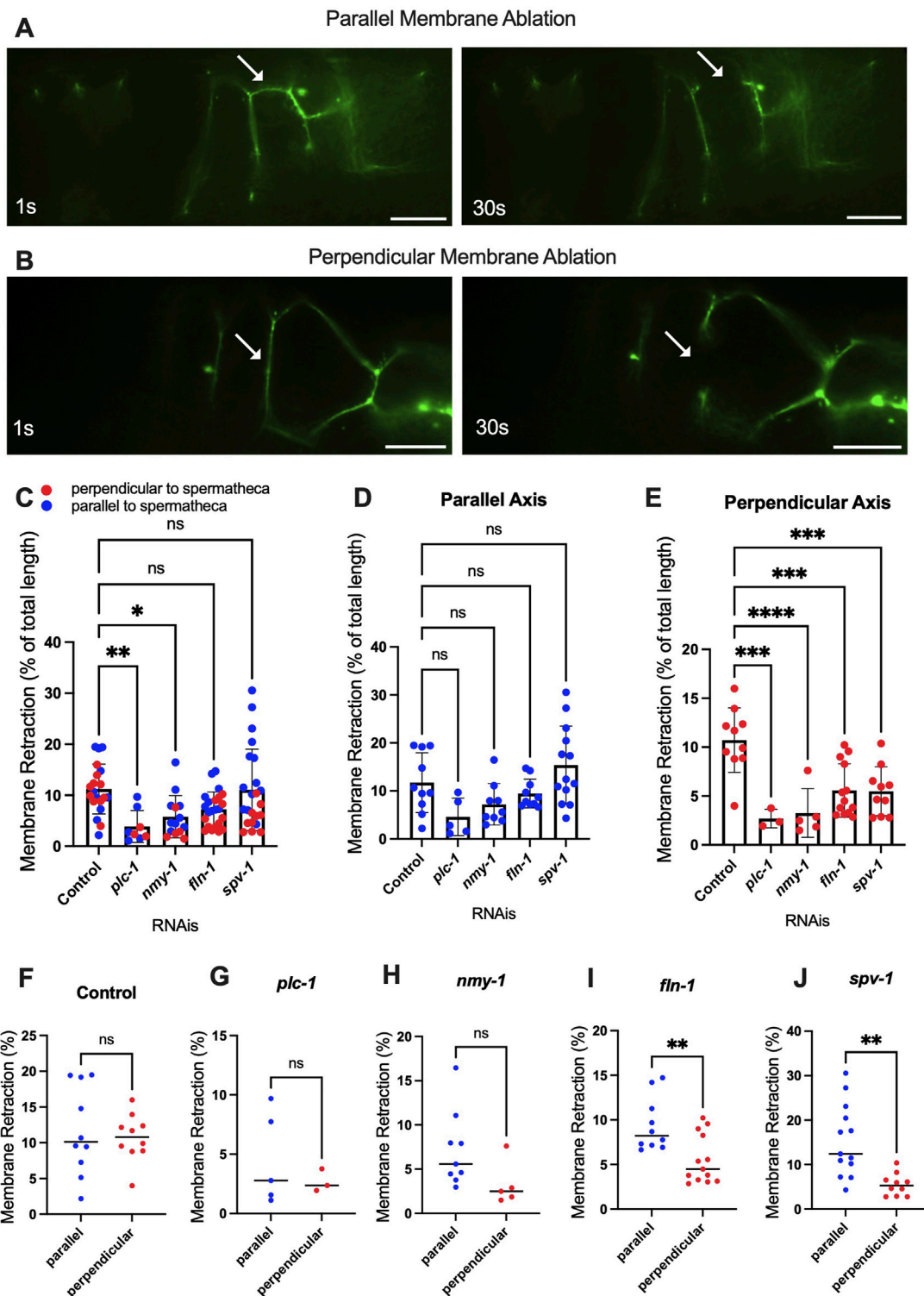
FIGURE 5
Altered contractility differentially affects severing of parallel and perpendicular apical junctions. Laser ablation of AJM-1::GFP expressing animals treated with control (empty vector) RNAi **(A, B)** before and 30 s after surgery (see *plc-1* RNAi, *nmy-1* RNAi, *fln-1* RNAi, and *spv-1* RNAi in Supplementary Figures S3, S4). Parallel **(A)** and perpendicular **(B)** membranes were severed using a femtosecond laser. **(C–E)** Percentage of the total retraction normalized to the length of the membrane indicates changes in tension on parallel **(D)** and perpendicular **(E)** membranes with *plc-1* RNAi, *nmy-1* RNAi, *fln-1* RNAi, and *spv-1* RNAi treatments compared to control **(F–J)**. Percentage of the total retraction normalized to the length of the membrane for each condition individually, comparing parallel and perpendicular membranes in control **(F)**, *plc-1* RNAi **(G)**, *nmy-1* RNAi **(H)**, *fln-1* RNAi **(I)**, and *spv-1* RNAi **(J)**. Retraction of control (empty vector) compared to other conditions using Ordinary one-way ANOVA, *****p < 0.0001*. Scale bar, 10 μm.

leading to decreased contractility. When *spv-1* is depleted by RNAi, the spermatheca is hypercontractile, often severing the oocytes upon entry or exit (Bouffard et al., 2019). As expected, actin fiber ablation in *spv-1* depleted animals shows an increase in fiber retraction, compared to controls (Figure 3C). We attempted to additionally increase tension in the spermatheca through depletion of the myosin phosphatase MEL-11. However, *mel-11* depletion resulted in spermathecal explosion due to excessive tension on fibers (Wirshing and Cram, 2017). The *spv-1* depletion result suggests activating myosin does increase tension on the basal actomyosin fibers.

3.3 Distention of the spermatheca does not significantly affect fiber tension

We observed that depletion of PLC-1 and NMY-1 leads to the entrapment of more than one embryo, distending the spermatheca. Conversely, spermathecae treated with *spv-1* RNAi are smaller than wildtype and often contain small pieces of oocytes due to increased contractility and severing of oocytes (Figure 2D). To quantify these effects, we measured the length and width of ACT-1::GFP expressing spermathecae in control and RNAi depleted animals, and saw significant increases in both length and width in the *plc-1* and *nmy-1* RNAi and significant decreases in length and width in *spv-1* RNAi treated animals compared to controls (Figures 4A, B). We next asked if there was a relationship between degree of distention of the spermatheca and tension on the actin fibers. Due to the imaging setup, it was not possible to measure the length or width of the spermatheca in the same animals in which fibers were severed. Therefore, we averaged the length and width of spermatheca from the data shown in Figures 4A, B, and plotted those averages against the average retraction of the actin fibers seen in the laser ablation experiments.

When PLC-1 and NMY-1 are depleted, the spermathecae are distended, and on average, there is slightly more tension on actin fibers, compared to the control condition. However, the fiber tensions in these RNAis are not significantly different from controls. In contrast, in *spv-1* RNAi treated animals with smaller spermatheca, the tension on actin is significantly increased (Figures 4C, D). These results suggest that the tension on the fibers does not scale with degree of distention of the tissue.

3.4 Apical cell junctions/membranes are under tension

Entry of the oocyte triggers actin rearrangement and actomyosin contractility (Bouffard et al., 2019). We speculated that tension on the cells of the spermatheca might also convey temporal or spatial information to inform the directional contraction that expels the fertilized embryo from the spermatheca. The circumferential actin fibers in the central spermathecal cells are not suitable for conveying lateral information. To address the question of whether mechanical information might be transmitted from cell to cell in the spermatheca, we first asked if the apical membranes and apical junction complexes might be under tension, and whether the tension differed in the parallel or perpendicular cell membranes.

To investigate tension along both axes of the cell membrane, we performed apical junction ablation parallel and perpendicular to the axis of the spermatheca in separate cells (Figures 5A, B), (Supplementary Movies S3, S4). We used laser severing to target the apical plasma membrane labeled with the apical junction marker AJM-1::GFP. In control conditions, the length of membrane retraction was similar in fibers parallel and perpendicular to the spermatheca (Figures 5C–F). However, when myosin contractility was reduced using *plc-1*, *nmy-1* and *fln-1* RNAi, we observed decreased membrane retraction in both parallel and perpendicular conditions compared to control, suggesting a decrease in membrane tension (Figure 5C). Most of this effect is the result of decreased membrane tension on fibers perpendicular to the axis of the spermatheca (compare Figures 5D, E). When we increased tension by depleting *spv-1,* we saw no overall change in the tension on apical membranes compared to control (Figure 5C), suggesting that most of the effect of SPV-1 is on the basal actomyosin fibers. However, we did observe a significant decrease in apical junction tension on perpendicular, but not parallel, apical membranes (Figures 5D, E). We also compared tensions on perpendicular *versus* parallel membranes for each gene depletion. No difference in tension was observed in control or the *plc-1* and *nmy-1* RNAi conditions (Figures 5F–H). Depletion of *fln-1*, which disrupts both the actin cytoskeleton and actomyosin contractility (Kelley et al., 2020) resulted in a significant decrease in tension on perpendicular membranes (Figure 5I). Depletion of *spv-1* also resulted in a significant decrease in tension on perpendicular membranes (Figure 5J). The *spv-1* results suggest increased contraction on the basal side of the spermatheca may reduce apical tension by compressing the tissue.

4 Discussion

In the spermatheca, actin and myosin are bundled into basal stress fiber-like actomyosin bundles. These bundles form during the initial ovulation and drive tissue contractility. We found that these fibers are under significant tension, influenced by both the presence of the oocyte and the activity of contractile proteins like SPV-1. Using laser ablation and RNA interference (RNAi), we demonstrate that decreasing contractility via depletion of *nmy-1*/myosin and *plc-1*/phospholipase C did not significantly affect fiber retraction, which suggests most of the tension on the fibers comes from the presence of the oocyte. While loss of PLC-1 does not strongly affect actin bundle formation, it leads to an absence of calcium release in the spermatheca, which is required for activation of myosin and contraction (Kovacevic et al., 2013). In contrast, increasing contractility by depleting SPV-1, which inactivates RHO-1, led to increased fiber retraction. This suggests that although the presence of the embryo strains the actomyosin fibers, activation of the Rho pathway can lead to further increases in contractility. It is also possible that occupancy causes the actin fibers to depolymerize at a faster rate upon severing. Pressure from the oocyte might cause an increase in the activity of actin depolymerizing proteins, such as UNC-60A (ADF/cofilin) (Ono and Benian, 1998).

The apical, lumen-facing surface of the spermathecal cells are connected with apical junctions. Apical junctions are also under tension in the occupied spermatheca. Reducing contractility decreases this tension. Perpendicular membranes are most strongly affected. This suggests that presence of the oocyte strains the width, or girth, of the spermatheca more than the length. This makes sense given the geometry of the spermatheca, which is a fairly narrow tube. We hypothesized that increasing contractility would increase tension on apical junctions as the tissue was pulled tightly against the egg. However, we found that when actomyosin contractility is increased through the depletion of SPV-1, apical tension is reduced. This suggests that increasing tension on the basal (outer) side of this biological tube compresses the inner the apical side. Depletion of SPV-1 and subsequent activation of RhoA may, as in other systems, also activate formins to promote the polymerization of actin (Sundaramurthy et al., 2020).

Laser ablation studies in other systems show actomyosin network and dynamics play a key role in the mechanical properties and morphologies of living cells (Fischer et al., 2014) (Beunk et al., 2022) (Hayward et al., 2021). Our work suggests the correct amount of tension is needed for tissue function. Similarly, in *C. elegans*, laser severing has been used to show CAP-1/actin capping protein limits myosin activity and cortical tension in the rachis of the hermaphrodite gonad (Ray et al., 2023). In *Drosophila* embryos, manipulation of myosin phosphorylation and actin polymerization give rise to changes in stiffness and contractility throughout the tissue, highlighting the importance of the cytoskeletal dynamics and transmitting contractile forces in developing tissues (Fischer et al., 2014). A laser severing study of wound healing in *Drosophila* embryos shows the necessity of myosin dynamics for stability and wound repair (Kobb et al., 2017). Cell and tissue shape have a significant influence on tensions. Similar to our observations, a study of tension and viscoelasticity of the sarcomere in single cells and in monolayers shows that the length and orientation of the stress fibers affect the retraction of the fibers (Kassianidou et al., 2017).

This study sheds light on the temporal dynamics of contractility and tension, the role of various cytoskeletal components, and how mechanical signals are integrated across the tissue to coordinate the complex process of oocyte transit. These findings enhance our understanding of the mechanical properties of reproductive tissues and the interplay between cellular structures and contractile proteins in regulating these properties.

Data availability statement

The original contributions presented in the study are included in the article/Supplementary Material, further inquiries can be directed to the corresponding author.

Author contributions

FS: Conceptualization, Investigation, Writing–original draft, Writing–review and editing. NG: Methodology, Writing–review and editing. SC: Resources, Writing–review and editing. EC: Conceptualization, Funding acquisition, Methodology, Resources, Writing–original draft, Writing–review and editing.

Funding

Acknowledgments

Conflict of interest

The authors declare that the research was conducted in the absence of any commercial or financial relationships that could be construed as a potential conflict of interest.

Publisher's note

All claims expressed in this article are solely those of the authors and do not necessarily represent those of their affiliated organizations, or those of the publisher, the editors and the reviewers. Any product that may be evaluated in this article, or claim that may be made by its manufacturer, is not guaranteed or endorsed by the publisher.

Supplementary material

The Supplementary Material for this article can be found online at: https://www.frontiersin.org/articles/10.3389/fcell.2024.1490803/full#supplementary-material

SUPPLEMENTARY FIGURE S1
Actin fiber ablation of ACT-1::GFP expressing animals treated with control **(A)**, *plc-1* **(B)**, *nmy-1* **(C)**, *spv-1* **(D)** RNAi. Scale bar, 10 μm.

SUPPLEMENTARY FIGURE S2
(A) Total actin retraction of ACT-1::GFP expressing animals treated with control, *plc-1* RNAi, *nmy-1* RNAi, *fln-1* RNAi, *spv-1* RNAi. **(B)** Total membrane retraction of AJM-1::GFP expressing animals treated with control, *plc-1* RNAi, *nmy-1* RNAi, *fln-1* RNAi, *spv-1* RNAi together, and separately [parallel **(C)** and perpendicular **(D)** membrane].

SUPPLEMENTARY FIGURE S3
Perpendicular membrane ablation of AJM-1::GFP expressing animals treated with control **(A)**, *plc-1* **(B)**, *nmy-1* **(C)**, *fln-1* **(D)**, *spv-1* **(E)** RNAis. Scale bar, 10 μm.

SUPPLEMENTARY FIGURE S4
Parallel membrane ablation of AJM-1::GFP expressing animals treated with control **(A)**, *plc-1* **(B)**, *nmy-1* **(C)**, *fln-1* **(D)**, *spv-1* **(E)** RNAis. Scale bar, 10 μm.

References

Ambrosini, A., Rayer, M., Monier, B., and Suzanne, M. (2019). Mechanical function of the nucleus in force generation during epithelial morphogenesis. *Dev. Cell.* 50 (2), 197–211. doi:10.1016/j.devcel.2019.05.027

Amiri, S., Muresan, C., Shang, X., Huet-Calderwood, C., Schwartz, M. A., Calderwood, D. A., et al. (2023). Intracellular tension sensor reveals mechanical anisotropy of the actin cytoskeleton. *Nat. Commun.* 14 (1), 8011. doi:10.1038/s41467-023-43612-5

Beunk, L., Bakker, G. J., van Ens, D., Bugter, J., Gal, F., Svoren, M., et al. (2022). Actomyosin contractility requirements and reciprocal cell–tissue mechanics for cancer cell invasion through collagen-based channels. *Eur. Phys. J. E* 45 (5), 48. doi:10.1140/epje/s10189-022-00182-6

Bouffard, J., Cecchetelli, A. D., Clifford, C., Sethi, K., Zaidel-Bar, R., and Cram, E. J. (2019). The RhoGAP SPV-1 regulates calcium signaling to control the contractility of the *Caenorhabditis elegans* spermatheca during embryo transits. *MBoC* 30 (7), 907–922. doi:10.1091/mbc.E18-10-0633

Castaneda, P. G., Cecchetelli, A. D., Pettit, H. N., and Cram, E. J. (2020). Gα/GSA-1 works upstream of PKA/KIN-1 to regulate calcium signaling and contractility in the *Caenorhabditis elegans* spermatheca. *PLoS Genet.* 16 (8), e1008644. doi:10.1371/journal.pgen.1008644

Chung, S. H., Clark, D. A., Gabel, C. V., Mazur, E., and Samuel, A. D. (2006). The role of the AFD neuron in *C. elegans* thermotaxis analyzed using femtosecond laser ablation. *BMC Neurosci.* 7 (1), 30. doi:10.1186/1471-2202-7-30

Colombelli, J., and Solon, J. (2013). Force communication in multicellular tissues addressed by laser nanosurgery. *Cell. Tissue Res.* 352 (1), 133–147. doi:10.1007/s00441-012-1445-1

Fischer, S. C., Blanchard, G. B., Duque, J., Adams, R. J., Arias, A. M., Guest, S. D., et al. (2014). Contractile and mechanical properties of epithelia with perturbed actomyosin dynamics. *PLOS ONE* 9 (4), e95695. doi:10.1371/journal.pone.0095695

Hayward, M. K., Muncie, J. M., and Weaver, V. M. (2021). Tissue mechanics in stem cell fate, development, and cancer. *Dev. Cell.* 56 (13), 1833–1847. doi:10.1016/j.devcel.2021.05.011

Kassianidou, E., Brand, C. A., Schwarz, U. S., and Kumar, S. (2017). Geometry and network connectivity govern the mechanics of stress fibers. *Proc. Natl. Acad. Sci.* 114 (10), 2622–2627. doi:10.1073/pnas.1606649114

Kelley, C. A., and Cram, E. J. (2019). Regulation of actin dynamics in the *C. elegans* somatic gonad. *J. Dev. Biol.* 7 (1), 6. doi:10.3390/jdb7010006

Kelley, C. A., Triplett, O., Mallick, S., Burkewitz, K., Mair, W. B., and Cram, E. J. (2020). FLN-1/filamin is required to anchor the actomyosin cytoskeleton and for global organization of sub-cellular organelles in a contractile tissue. *Cytoskeleton* 77 (10), 379–398. doi:10.1002/cm.21633

Kelley, C. A., Wirshing, A. C. E., Zaidel-Bar, R., and Cram, E. J. (2018). The myosin light-chain kinase MLCK-1 relocalizes during *Caenorhabditis elegans* ovulation to promote actomyosin bundle assembly and drive contraction. *MBoC* 29 (16), 1975–1991. doi:10.1091/mbc.E18-01-0056

Kobb, A. B., Zulueta-Coarasa, T., and Fernandez-Gonzalez, R. (2017). Tension regulates myosin dynamics during Drosophila embryonic wound repair. *J. Cell. Sci.* 130 (4), 689–696. doi:10.1242/jcs.196139

Kovacevic, I., and Cram, E. J. (2010). FLN-1/Filamin is required for maintenance of actin and exit of fertilized oocytes from the spermatheca in *C. elegans*. *Dev. Biol.* 347 (2), 247–257. doi:10.1016/j.ydbio.2010.08.005

Kovacevic, I., Orozco, J. M., and Cram, E. J. (2013). Filamin and phospholipase C-ε are required for calcium signaling in the *Caenorhabditis elegans* spermatheca. *PLOS Genet.* 9 (5), e1003510. doi:10.1371/journal.pgen.1003510

Mateos, C. S. C., Valencia-Expósito, A., Palacios, I. M., and Martín-Bermudo, M. D. (2020). Integrins regulate epithelial cell shape by controlling the architecture and mechanical properties of basal actomyosin networks. *PLOS Genet.* 16 (6), e1008717. doi:10.1371/journal.pgen.1008717

Ono, S., and Benian, G. M. (1998). Two *Caenorhabditis elegans* actin depolymerizing factor/cofilin proteins, encoded by the *unc-60* gene, differentially regulate actin filament dynamics. *J. Biol. Chem.* 273 (6), 3778–3783. doi:10.1074/jbc.273.6.3778

Ray, S., Agarwal, P., Nitzan, A., Nédélec, F., and Zaidel-Bar, R. (2023). Actin-capping protein regulates actomyosin contractility to maintain germline architecture in *C. elegans*. *Development* 150 (6), dev201099. doi:10.1242/dev.201099

Sundaramurthy, S., Votra, S., Laszlo, A., Davies, T., and Pruyne, D. (2020). FHOD-1 is the only formin in *Caenorhabditis elegans* that promotes striated muscle growth and Z-line organization in a cell autonomous manner. *Cytoskelet. Hob.* 77 (10), 422–441. doi:10.1002/cm.21639

Tan, P. Y., and Zaidel-Bar, R. (2015). Transient membrane localization of SPV-1 drives cyclical actomyosin contractions in the *C. elegans* spermatheca. *Curr. Biol.* 25 (2), 141–151. doi:10.1016/j.cub.2014.11.033

Taneja, N., Bersi, M. R., Rasmussen, M. L., Gama, V., Merryman, W. D., and Burnette, D. T. (2020). Inhibition of focal adhesion kinase increases myofibril viscosity in cardiac myocytes. *Cytoskeleton* 77 (9), 342–350. doi:10.1002/cm.21632

Wang, Y. L., Grooms, N. W. F., and Chung, S. H. (2022). Transverse and axial resolution of femtosecond laser ablation. *J. Biophot.* 15 (9), e202200042. doi:10.1002/jbio.202200042

Wirshing, A. C. E., and Cram, E. J. (2017). Myosin activity drives actomyosin bundle formation and organization in contractile cells of the *Caenorhabditis elegans* spermatheca. *Mol. Biol. Cell.* 28 (14), 1937–1949. doi:10.1091/mbc.E17-01-0029

Wirshing, A. C. E., and Cram, E. J. (2018). Spectrin regulates cell contractility through production and maintenance of actin bundles in the *Caenorhabditis elegans* spermatheca. *MBoC* 29 (20), 2433–2449. doi:10.1091/mbc.E18-06-0347